EFFECT OF SATURATION HISTORY ON THREE-PHASE RELATIVE PERMEABILITY: AN EXPERIMENTAL STUDY

A.H. Alizadeh and M. Piri
Department of Chemical & Petroleum Engineering, University of Wyoming, Dept. 3295, 1000 E. University Ave., Laramie, WY 82071-2000, USA

This paper was prepared for presentation at the International Symposium of the Society of Core Analysts held in Napa Valley, California,, USA, 16-19 September, 2013

ABSTRACT

Simultaneous flow of three fluid phases, e.g., oil, gas, and brine, in porous media is of great interest in many areas of science and technology, such as petroleum reservoir and environmental engineering. Among all properties of three-phase flow through porous media, relative permeability is one of the most important and least understood ones. While the importance of three-phase relative permeability has long been recognized, only a few reliable, well-characterized experimental studies are available in the literature. In this study we present a unique world-class three-phase flow and computed tomography experimental apparatus designed for simultaneous injection and recirculation of all fluid phases in a closed loop at reservoir conditions. We utilize the setup to perform steady-state flow tests to study two- and three-phase relative permeabilities. The experiments are performed through vertically-placed Bentheimer sandstone core samples in a core holder with multiple pressure ports. We use brine/Soltrol 170/nitrogen fluid system. In particular, we investigate the effect of different saturation histories (relevant to various oil displacement processes, including secondary and tertiary gas injections) on the stability of spreading oil layers and residual oil saturation. The functional forms of oil (intermediate-wetting phase) relative permeability with saturation, particularly at low oil saturations, are examined. It is observed that at high oil saturations, where networks of pores filled with oil govern oil flow, oil relative permeability exhibits a quartic form with oil saturation ($k_{ro} \sim S_o^4$), whereas at low oil saturations, it shows a quadratic form ($k_{ro} \sim S_o^2$). The quadratic form of three-phase oil relative permeability is consistent with the theoretical interpretation of layer drainage at the pore scale. These experimentally-measured relative permeability data can be used to validate and also develop physically-based pore-scale models of two- and three-phase flow.

INTRODUCTION

Simultaneous flow of three phases is encountered often enough in petroleum reservoirs and during non-aqueous phase migration to warrant a detailed study of the process. Among the parameters that influence three-phase flow, relative permeability probably has the uttermost role. While the importance of three-phase relative permeability has long been recognized, it has not received much attention as it merits. Work on three-phase

relative permeability was commenced nearly seven decades ago by Leverett and Lewis [1] in 1941; however, it was not able to grow in experimentation as properly as two-phase relative permeability, mainly due to the difficulties and complexities associated with its experimental measurements. A review of experimental studies on three-phase relative permeability [2] demonstrates that there are solely fewer than hundred published papers on this subject against numerous papers on two-phase relative permeability. This underdevelopment, therefore, has led to little understanding of pore-level displacement physics involved and their consequences on three-phase flow.

For a given rock-fluid system and under fixed experimental conditions, relative permeabilities are not unique functions of phase saturations, but may depend upon saturation history as well. Saraf *et al.* [3] measured two- and three-phase relative permeabilities in water-wet fired Berea sandstone using both the steady- and unsteady-state methods under similar saturation histories. Three-phase unsteady-state gas relative permeability was found to be a function of gas saturation and gas saturation history. Three-phase gas relative permeabilities of the steady-state experiments, however, were less sensitive to gas saturation history. Three-phase relative permeability to water was only a function of water saturation and almost independent of saturation history. In the case of relative permeability to oil, the three-phase data were not strongly dependent on the direction of saturation change of liquid phases, but influenced by the gas saturation history. Maini *et al.* [4] carried out a series of steady-state relative permeability experiments on a water-wet sandpack at elevated temperature. It was observed that, despite considerable scatter, three-phase water relative permeability depended only on water saturation. Gas relative permeability was also a function of only gas saturation in each saturation history. Three-phase relative permeability to oil also showed some hysteresis and was found to vary with the other phase saturations as well. Oak [5] measured two- and three-phase relative permeabilities in water-wet fired Berea sandstone cores for a large number of saturation histories. It was reported that three-phase permeability to water was mainly a function of water saturation. Three-phase gas relative permeabilities depended mainly on gas saturation as well as the direction of gas saturation change. Three-phase relative permeability to oil varied with all saturations. The variation depended upon saturation history.

Formation of spreading oil layers sandwiched between water and gas in water-wet and mixed-wet pores is an important feature of three-phase flow through porous media. Flow of oil through these spreading layers, even though slowly, can lead to very low oil saturations, thereby improving recovery efficiency [6]. While spreading and layer flow are not new concepts in fluid flow in porous media and a large number of studies have focused on their influences on residual oil saturation and recovery efficiency, only a few studies [7,8] have been dedicated to examination of layer flow on three-phase relative permeabilities under different saturation histories. Sahni *et al.* [7] performed a series of secondary and tertiary gas gravity drainage experiments on a water-wet uniform sandpack and a water-wet Berea sandstone core under various initial saturation conditions. For sand, oil relative permeability was primarily a function of oil saturation

and independent of initial conditions; however, the functionality was different depending upon the spreading coefficient. In general, $k_{ro} \sim S_o^a$ that *a* varied with the spreading coefficient as well as the range of oil saturation. At high oil saturations, i.e., oil saturations higher than waterflood residual oil, *a* was about 4 for both spreading and non-spreading fluid systems whereas, at oil saturations lower than waterflood residual oil, *a* was around 2 only for spreading oils. Similar results were also reported by DiCarlo *et al.* [8] for water-wet sandpacks. The observed functional forms were believed not to be universal and to depend upon the porous medium.

In this study, we investigate the effect of different saturation histories (relevant to various oil displacement processes, including secondary and tertiary gas injections) on three-phase gas/oil/brine relative permeabilities of water-wet consolidated Bentheimer sandstone and on the stability of spreading oil layers and residual oil saturation. The functional forms of oil (intermediate-wetting phase) relative permeability with saturation, particularly at low oil saturations, are also examined.

CORE SAMPLES AND FLUIDS

Two core plugs, 6 inches in length and 1.5 inches in diameter, were cut from a block of Bentheimer sandstone using tap water as a coolant, dried in an oven at 110°C for 3 days and cooled in a desiccator for 2 days. The plugs (Sample 12 and Sample 13) were then X-ray imaged to investigate their homogeneity. The three-dimensional images of the samples demonstrated that they were homogeneous. Brine permeabilities of Samples 12 and 13 were 2.40 and 2.44 D, respectively, and their average porosities determined using X-ray imaging were 24.1 and 24.7%, respectively. Figure 1 shows the distribution of porosity along the length of the Bentheimer core samples.

The aqueous phase was formulated using distilled water, 2 wt% $CaCl_2$, 12 wt% NaI, and 0.01 wt% NaN_3. Sodium azide was added to brine to avoid bacterial growth. Brine density was 1.1381 g/cm^3 at 800 psig and 25°C. A low-salinity brine containing 1.5 wt% $CaCl_2$ was utilized as a buffer between the working aqueous phase and cleaning solvents, when necessary. Soltrol 170 (a mineral oil) was purified by passing it through a dual-packed column of silica gel and alumina to remove polar contaminants, which might alter the water wetness of the rock, and then iodooctane (5 vol%) was dissolved in the purified Soltrol to obtain a working oil phase of density equal to 0.8002 g/cm^3 at 800 psig and 25°C. Sodium iodide and iodooctane were added as X-ray dopants to the aqueous and oil phases, respectively. All chemicals were reagent grade and used as received. Commercial N_2 was used as the gas phase. It was withdrawn from a pressurized cylinder. In the rock-fluid system selected, the aqueous, oil, and gas phases were the most wetting, intermediate-wetting, and non-wetting phases, respectively. The aqueous and oil phases are hereafter referred to as water and oil, unless stated otherwise.

Interfacial tensions between pairs of phases were measured at equilibrium, i.e., in the presence of the third phase, using the pendant drop technique. The IFT values of the nitrogen-brine, nitrogen-oil, and oil-brine pairs were 61.7136, 20.9568, and 40.7656

mN/m, respectively. Thus, the equilibrium spreading coefficient for the fluid system used in this study was zero, implying the oil phase would spread on the aqueous phase in the presence of the gas phase and flow through spreading layers.

EXPERIMENTAL APPARATUS

The apparatus was originally designed for three-phase relative permeability measurements under full fluid re-circulation, but was so modular that could be utilized for determining other fluid flow properties, capillary pressures for instance, and also examining a variety of different enhanced oil recovery techniques [9]. The coreflooding setup was a closed-loop system composed of dual-cylinder Quizix™ pumps, Rosemount™ differential pressure transducers, Cambridge™ fluid viscometers, a Hassler-type multi-pressure-port core holder constructed from Aluminum, a 3500-cm^3 three-phase separator, compensation accumulators, mechanical convection ovens, and a dual-oriented medical X-ray CT scanner for in-situ saturation measurements. Figure 2 shows a detailed schematic diagram of the setup. All parts of the apparatus exposed to flooding fluids were made of Hastelloy™ and other corrosion-resistant materials.

The dual-cylinder pumps were used for injection of three fluids, i.e., brine, oil, and gas (Pumps 1 to 3), back pressure regulation (Pump 4), overburden pressure maintenance (Pump 5), and separator pressure regulation (Pump 6). The fluids were simultaneously injected into the core samples at constant flow rates using Pumps 1 to 3. The injection pumps withdrew their respective fluids for re-injection into the core samples from appropriate locations designated on the separator. The fluids produced from the cores were received by Pump 4 in paired constant-pressure receive mode. This approach allowed imposing a constant-pressure boundary condition at the outlet of the cores and maintaining stable back pressures, as opposed to customary back pressure regulators, even at high flow rates. Pump 4 discharged its fluids, received from the core, into the separator. Retracting the injection fluids from and delivering the effluent fluids to the separator provided full fluid re-circulation. This capability not only created much more stable equilibrium between the phases throughout experiments, but also reduced the need for additional fluids. Prior to the start of an experiment, all fluids were also re-circulated through the apparatus, albeit by bypassing the core holder, for a sufficiently long period of time in order to achieve equilibrium between the phases and minimize interphase mass transfer during experiments. Injection of fluids into the separator by the back pressure regulation pump and intermittent withdrawal of fluids by the injection pumps could in principle lead to considerable variations in pressure of the separator, particularly at high flow rates, even though the volume of the separator was relatively large (3500 cm^3). To reduce such effects, a separator pressure regulation system compensated for all the accumulations (positive or negative) using a large dual-cylinder pump (Pump 6) that allowed us to obtain very stable separator pressures leading to stable equilibrium between fluids. Pressure drop measurements were made across the middle part of the core samples (4 inches) to reduce capillary end effects. For better precision over a broad range of pressure drop, three differential transducers with various ranges were connected in parallel together, and each was selected during a flow test on the basis of the pressure

drop value. A sophisticated control system was utilized to operate the pumps and log the data throughout the experiments. Finally, the medical CT scanner used could be rotated from horizontal to vertical orientation allowing flow tests through vertically- and horizontally-placed core samples.

EXPERIMENTAL PROCEDURE

A series of constant-flow-rate steady-state two- and three-phase relative permeability experiments were performed on two vertically-oriented water-wet Bentheimer core samples using a brine/Soltrol 170/nitrogen fluid system at 20°C and 800 psig back pressure. A net overburden pressure of 250 psi was applied during all displacements, and all fluid phases were injected from the bottom of the sample. In the experiments performed, the magnitude of Bond number was always low, in the order of 10^{-6}, indicating that gravity effects were insignificant. This was confirmed by uniform saturation distributions along the cores in all experiments. Also, all displacements were capillary-controlled at the pore scale; i.e. the capillary number was about 10^{-6}. Below, we present the experimental procedure in more detail.

In-situ Saturation Measurement

As mentioned already, three-phase saturations in this study were measured in-situ using computed tomography. To calculate three phase saturations, the cores were scanned at two different energy levels during the experiments and also when they were fully saturated with each of the fluids (to obtain reference scans). Saturations were then determined by obtaining a simultaneous solution for the following system of equations:

$$S_w = \frac{(CT_{c2} - CT_{gc2})(CT_{oc1} - CT_{gc1}) - (CT_{c1} - CT_{gc1})(CT_{oc2} - CT_{gc2})}{(CT_{oc1} - CT_{gc1})(CT_{wc2} - CT_{gc2}) - (CT_{oc2} - CT_{gc2})(CT_{wc1} - CT_{gc1})} \quad (1)$$

$$S_o = \frac{(CT_{c1} - CT_{gc1})(CT_{wc2} - CT_{gc2}) - (CT_{c2} - CT_{gc2})(CT_{wc1} - CT_{gc1})}{(CT_{oc1} - CT_{gc1})(CT_{wc2} - CT_{gc2}) - (CT_{oc2} - CT_{gc2})(CT_{wc1} - CT_{gc1})} \quad (2)$$

$$S_g = 1 - S_w - S_o \quad (3)$$

where CT_{c1} and CT_{c2} are the CT numbers of the core containing all phases at energy levels 1 and 2, respectively. The saturation measurements were carried out by scanning the middle part of the samples (4 inches - between the two middle pressure ports) at two different energy levels. The lower energy was at 80 keV and the higher energy was at 130 keV. Each slice had a thickness of 2 mm and the distance between two consecutive slices was 4 mm. CT images affected by the metal pressure ports were excluded from saturation calculations. Fluid saturations were determined at 21 locations equidistant along the core axis and then averaged to report one value for each phase. In two-phase water-oil experiments (prior to any gas injection), dual-energy scanning resulted in gas saturations of about ± 0.01. Therefore, the accuracy of the measured saturations in this study was estimated to be 1%.

Porosity Measurement

Porosity was calculated from

$$\varphi = \frac{CT_{wc} - CT_{gc}}{CT_w - CT_g} \quad (4)$$

where CT_{wc} and CT_{gc} are CT numbers of the core fully saturated with brine and gas, respectively. CT_w and CT_g were obtained by scanning the core holder filled with only brine or gas, respectively.

Controlling Saturation Histories

In steady-state three-phase relative permeability experiments, similar to two-phase, all phases are flowed together through the sample at a set of fixed fractional flows until steady state is reached, before moving to the next set of fractional flows. Selection of the next set of fractional flows must be made with special care to follow the saturation history being investigated and to avoid any unwanted irreversible switch between drainage and imbibition displacement processes.

In cases where only two phases are injected, the control of saturation histories is straightforward because any changes (decrease or increase) in the flow rate of one of the phases corresponds to a change in its saturation in the same direction and a change in the saturation of the other injected phase in the opposite direction. In cases where all three phases are simultaneously injected, however, there is no such a correlative relationship between the direction of flow rate change and saturation. In other words, the flow rate and saturation of a phase may vary in opposite directions, depending on how other flow rates are changed. When three mobile phases are present, only two saturations can vary in the same direction and the third one has to obviously change in the other direction due to material balance constraints. This simple fact can inspire an approach in which two phases that their saturations change in the same direction are grouped together and treated as a single phase. In this way, the three-phase flow problem is simplified to a two-phase problem, meaning that saturation histories of two- and three-phase relative permeability experiments can be controlled in a similar manner. In a steady-state oil-displacing-water two-phase test, for example, where oil saturation increases and water saturation decreases, the saturation history is driven by decreasing the water flow rate and/or increasing the oil flow rate at each step so that the ratio of oil to water flow rate follows a monotonically ascending path throughout the test. The same approach can be applied for three-phase flow. For example, in a three-phase test where water and oil saturation decrease and gas saturation increases, the saturation history is controlled by increasing the gas flow rate and/or decreasing both oil and water flow rates concurrently, while maintaining the water to oil fractional flow ratio.

Criteria for a Steady-state Condition

During steady-state relative permeability experiments, the system was allowed to reach steady state at each set of fixed fractional flows before moving to the next set. Steady state was judged from constant fluid saturations and stable pressure drop along the sample. Simple application of the multiphase version of Darcy's law to each phase then

yielded relative permeabilities. In this study, steady state was assumed to have been attained when pressure fluctuations were less than 1% over 30 minutes and saturation variations were less than 1% in two hours.

Cleaning the Core Samples

After completion of each series of tests, the core samples were cleaned for subsequent experiments. In three-phase flow where water, oil, gas are present, flushing the medium directly with solvents may not be sufficiently efficient because the gas phase does not usually get dissolved in them at low pressures. Accordingly, the gas phase, N_2, was displaced with CO_2, which was greatly soluble in water (brine), and then CO_2 was in turn displaced with several pore volumes of low-salinity brine (containing 1.5 wt% $CaCl_2$) at moderate pore pressures. Once only brine and oil remained in the pore space, the core was flushed with 20 pore volumes of isopropanol and then oven dried. The low-salinity brine was employed to avoid salt precipitation between the high-salinity brine used in the experiments and isopropanol.

RESULTS AND DISCUSSION

In this study, we investigated the effect of saturation history on three-phase relative permeability in a water-wet sandstone with a brine/Soltrol/nitrogen fluid system. Soltrol was spreading on brine in the presence of nitrogen. We performed two steady-state secondary gas injection experiments (SGI) after primary oil injection and one steady-state tertiary gas injection (TGI) after waterflooding. The SGI floods had different initial oil saturations (i.e., 90 and 65%) while the TGI test was performed with initial oil saturation similar to that of the second SGI (i.e., 70%). Figure 3 presents the saturation paths taken by these three experiments. In the first SGI, gas displaces only oil at connate water saturation (S_{wi}) generating a saturation path with constant water saturation. Before gas invasion into oil, majority of the pores (with the exception of very small elements) hosted oil in the center and brine in the corners (see Figure 4(a)). Displacement of oil by gas leads to formation of spreading oil layers sandwiched between gas in the center and brine in the corner (see Figures 4(b) and 5). The three-phase oil relative permeability during this process at high oil saturations ($S_o > S_{or}^{wf}$) is controlled by flow of bulk oil through the center of the pores. At low oil saturations, however, flow through the oil layers controls the relative permeability. The stability of these oil layers is affected by interfacial tensions, the spreading coefficient, wettability (i.e., oil/water, gas/water, and gas/oil contact angles), and oil/water and gas/oil capillary pressures. During gas injection, and for a given rock-fluid system, oil layers are stable over a wider range of gas/oil capillary pressure if the test is carried out with a higher initial oil/water capillary pressure (i.e., higher S_{oi}). More stable oil layers allow gas injection to reach lower residual oil saturation. At high gas/oil capillary pressures (late stages of gas injection), oil layers will collapse forming fluid configuration (c) shown in Figure 4. Our first SGI with initial oil saturation (S_{oi}) of 0.9 led to residual oil saturation of 0.108. Figures 6, 7, and 8 present the three-phase water, gas, and oil relative permeabilities. For comparison, we have also included two-phase oil/water counterparts.

With the second SGI flow test, we examined the impact of lower S_{oi} (i.e., 0.65) on the relative permeabilities. As shown in Figure 3, gas displaces both brine and oil leading to residual oil saturation of 0.145. In this test, we established a smaller, compared to the first SGI, oil/water capillary pressure before the onset of gas injection. This reduces the stability of the spreading oil layers allowing them to collapse at lower gas/oil capillary pressures, which in turn leads to a higher residual oil saturation (i.e., 0.145). The third three-phase flow test included gas injection after a partial waterflood. Prior to gas injection, a steady-state waterflood step was used to establish an initial oil saturation of 0.7. A subsequent gas injection led to residual oil saturation of 0.173, higher than those of two SGI experiments reported earlier. This is again attributed to a) the impact of lower initial oil/water capillary pressure, caused by the preceding waterflood, on the stability of the spreading oil layers, and b) oil/water contact angle hysteresis associated with the oil/water interface in Figure 4(b). The interface will have greater contact angle (than receding value) due to waterflood, which could impact the stability of the oil layer during the subsequent gas injection.

From Figure 6, it is evident that water relative permeability is a function of only water saturation as two-phase and three-phase curves follow the same trend. This is expected as water is the most wetting phase and occupies the smallest pores. In other words, saturation history has a limited impact on the distribution of pore sizes occupied by water. Gas relative permeability exhibits a similar behavior, i.e., it depends only on gas saturation (Figure 7). This is also expected as gas is the most non-wetting phase and therefore occupies the largest pores in the medium. Gas pore occupancy is mainly controlled by the gas saturation. This does not mean that gas relative permeability is not sensitive to the direction of gas saturation change. As the most non-wetting phase, its relative permeability is expected to exhibit hysteresis should the gas saturation decreases due imbibition processes such as water injection.

The three-phase oil relative permeability curves show relatively weak sensitivity to variations in initial oil saturation. This is attributed to narrow pore size distribution of Bentheimer sandstone limiting the range of pore sizes that oil can occupy due to various saturation histories. As the intermediate-wetting phase, it is generally expected the oil relative permeability to be a function of two saturations (e.g., oil and gas). However, for decreasing oil saturation in the system studied, we observe that three-phase oil relative permeability is mainly a function of oil saturation. Oil relative permeability may also exhibit different trends with the direction of oil saturation change (i.e., decreasing vs. increasing). This effect called relative permeability hysteresis requires more experiments in which oil saturation increases. In Figure 8, primary oil drainage relative permeability shows a distinctly different trend than those of gas injection experiments. This is because during primary drainage, oil occupies the largest pores while during gas injection oil resides only in intermediate size pores. Figure 9 shows the functional forms of oil (intermediate-wetting phase) relative permeability with saturation. It is observed that at high oil saturations, where networks of pores filled with oil dominate flow of oil, oil relative permeability exhibits a quartic form with oil saturation ($k_{ro} \sim S_o^4$), whereas at low

oil saturations, it shows a quadratic form ($k_{ro} \sim S_o^2$). The quadratic form of three-phase oil relative permeability is consistent with the theoretical interpretation of layer drainage at the pore scale, i.e., $A_o \sim S_o$, $g_o \sim A_o^2$, and $k_{ro} \sim g_o$, therefore $k_{ro} \sim S_o^2$, where A_o, g_o, and k_{ro} are cross-sectional area, hydraulic conductivity, and relative permeability of oil layer in a corner (see Figure 4(b)).

CONCLUSIONS

Steady-state three-phase gas injection experiments were performed with various initial oil saturations to investigate the impact of saturation history on three-phase oil, water, and gas relative permeabilities as well as ultimate residual oil saturation. Water and gas relative permeabilities were found to be functions of their own saturations only, while oil relative permeability showed weak sensitivity to initial oil saturation. It is observed that oil relative permeability exhibits a quartic form with oil saturation ($k_{ro} \sim S_o^4$) at high oil saturations, whereas at low oil saturations, it shows a quadratic form ($k_{ro} \sim S_o^2$).

ACKNOWLEGMENT

We gratefully acknowledge financial support of EnCana, Saudi Aramco, the School of Energy Resources and the Enhanced Oil Recovery Institute at the University of Wyoming.

REFERENCES

1. Leverett, M.C. and W.B. Lewis, "Steady Flow of Gas-oil-water Mixtures through Unconsolidated Sands," *Trans. AIME*, (1941) **142**, 1, 107-116.
2. Alizadeh, A.H. and M. Piri, "Three-Phase Flow in Porous Media: A Review of Experimental Studies of Relative Permeabilities," Submitted to *Reviews of Geophysics*.
3. Saraf, D.N., J.P. Batycky, C.H. Jackson and D.B. Fisher, "An Experimental Investigation of Three-Phase Flow of Water-Oil- Gas Mixtures Through Water-Wet Sandstones," paper SPE 10761 presented at the SPE Regional Meeting, San Francisco, California, 24-26 March, 1982.
4. Maini, B.B., S. Kokal and K. Jha, "Measurements and Correlations of Three-Phase Relative Permeability at Elevated Temperatures and Pressures," paper SPE 19677 presented at the 64th SPE Annual Technical Conference and Exhibition, San Antonio, Texas, 8-11 October, 1989.
5. Oak, M.J, "Three-phase Relative Permeability of Water-wet Berea," paper SPE 20183 presented at the SPE/DOE Seventh Symposium on Enhanced Oil Recovery, Tulsa, Oklahoma, 22-25 April, 1990.
6. Vizika, O. and J.-M. Lombard, "Wettability and Spreading: Two Key Parameters in Oil Recovery With Three-Phase Gravity Drainage," *SPE Reservoir Engineering*, (1996) **11**, 1, 54-60.
7. Sahni, A., J. Burger and M.J. Blunt, "Measurement of Three Phase Relative Permeability During Gravity Drainage Using CT Scanning," paper SPE 39655

presented at the SPE/DOE Improved Oil Recovery Symposium, Tulsa, Oklahoma, 19-22 April, 1998.
8. DiCarlo, D.A., A. Sahni and M.J. Blunt, "Three-Phase Relative Permeability of Water-Wet, Oil-Wet, and Mixed-Wet Sandpacks," *SPE Journal*, (2000) **5**, 1, 82-91.
9. Piri, M., "Recirculating, Constant Backpressure Core Flooding Apparatus and Method," US Patent No. WO 2012/082797 A1, 2012.

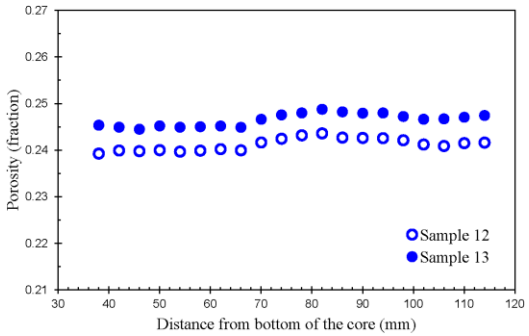

Figure 1. Slice-averaged porosity distribution along the length of the Bentheimer core samples determined using X-ray imaging.

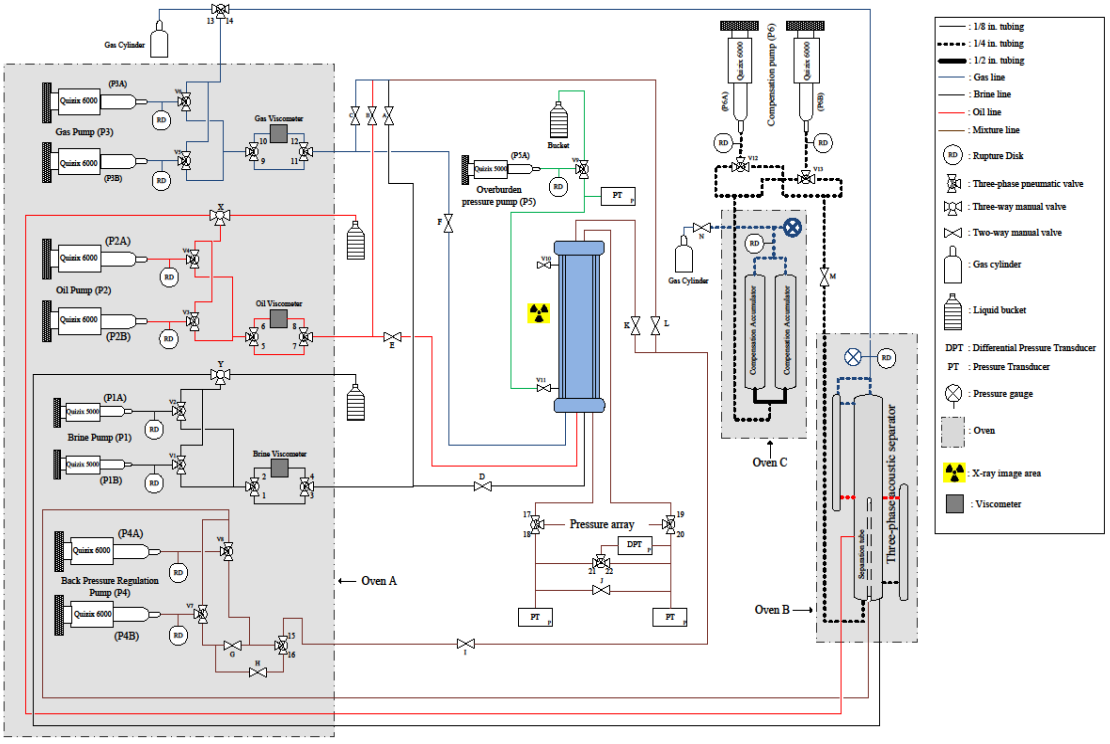

Figure 2. Schematic diagram of the three-phase coreflooding setup [9].

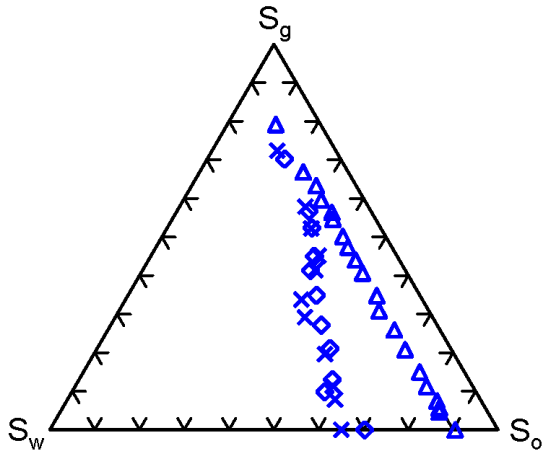

Figure 3. Saturation trajectories; Δ and x: secondary gas injections (S_{oi} = 90 and 65%, respectively), and ◊: tertiary gas injection (S_{oi} = 70%).

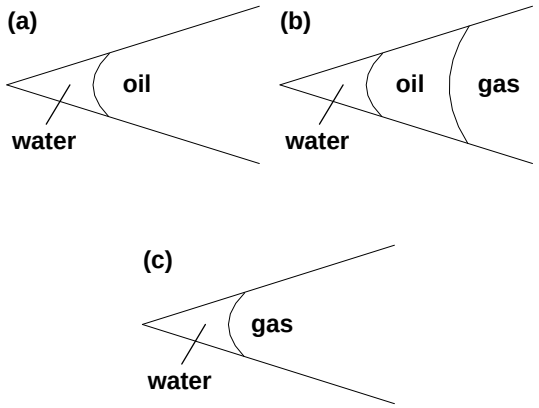

Figure 4. Corner fluid configurations in pores with angular cross section for: (a) primary oil drainage, (b) gas injection, and (c) at the end of gas injection.

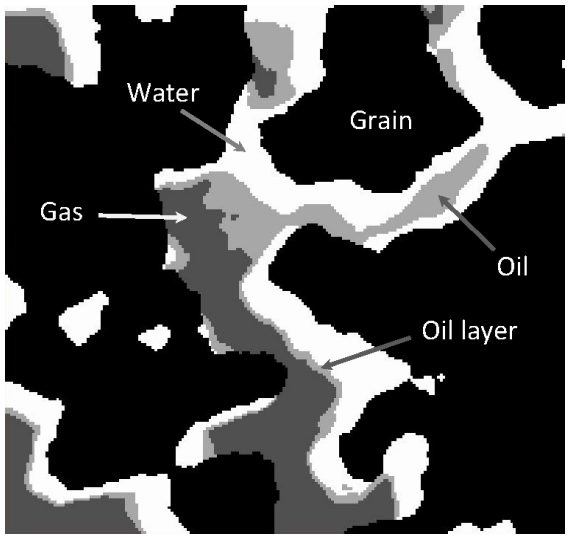

Figure 5. A segmented three-phase pore-scale fluid occupancy map obtained using a high-resolution micro-tomography system (medium: Bentheimer sandstone; fluids: brine (16.5 wt% NaI), oil (Soltrol 170 + 1.5 vol% iodooctane), gas (nitrogen); resolution: 3 microns).

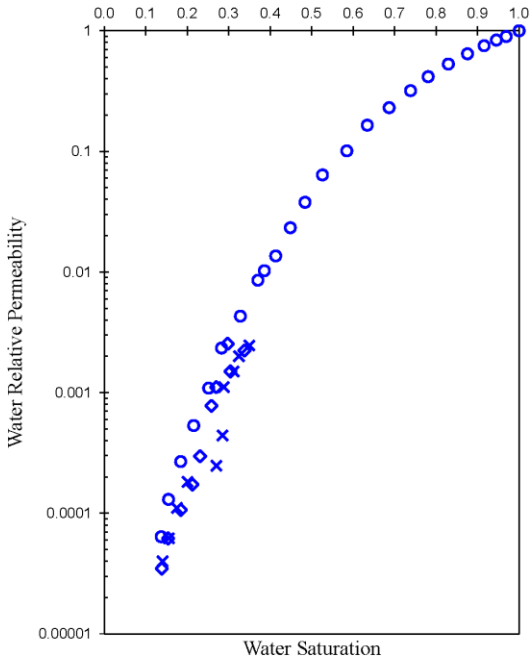

Figure 6. Water relative permeability; ○: two-phase relative permeabilities in water/oil drainage, x: secondary gas injection (S_{oi} = 65%), and ◊: tertiary gas injection (S_{oi} = 70%).

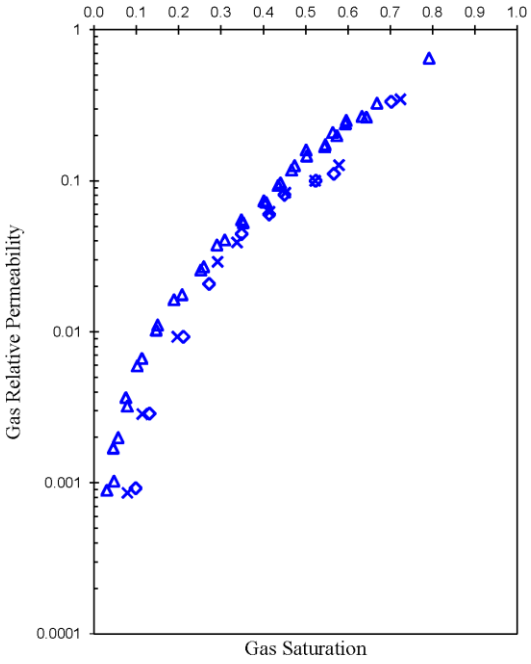

Figure 7. Gas relative permeability; Δ and x: secondary gas injections (S_{oi} = 90 and 65%, respectively), and ◊: tertiary gas injection (S_{oi} = 70%).

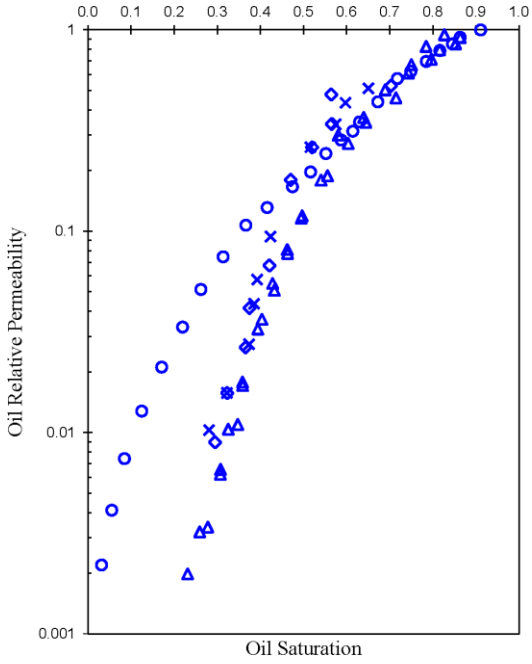

Figure 8. Oil relative permeability; ○: two-phase relative permeabilities in water/oil drainage, Δ and x: secondary gas injections (S_{oi} = 90 and 65%, respectively), and ◊: tertiary gas injection (S_{oi} = 70%).

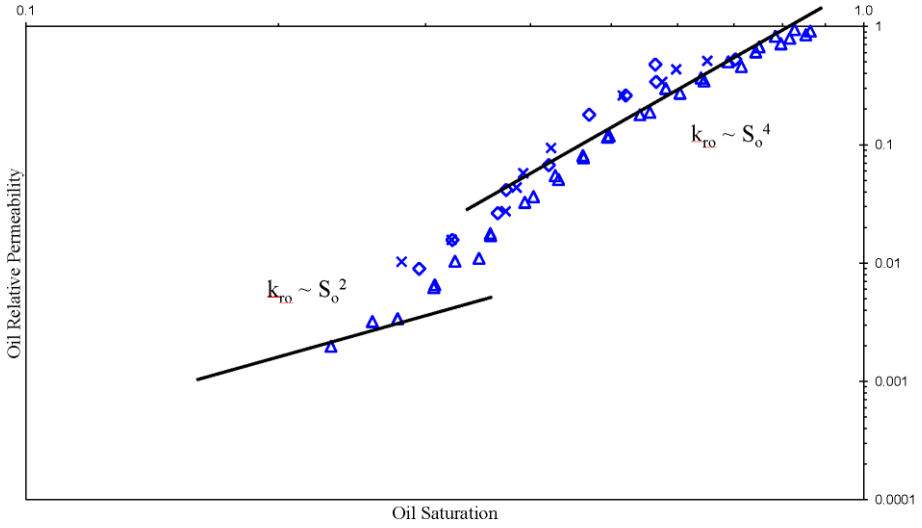

Figure 9. At high oil saturations, oil relative permeability is governed by the network of pores filled with oil and $k_{ro} \sim S_o^4$. At low oil saturations, where flow is controlled by layer drainage, $k_{ro} \sim S_o^2$.